ELSEVIER

Contents lists available at ScienceDirect

## **Ecological Indicators**

journal homepage: www.elsevier.com/locate/ecolind



## Original Articles



# Impact of future climate warming on soil organic carbon stocks in Inner Mongolia, China

Shuai Wang <sup>a,b,c</sup>, Xingyu Zhang <sup>a</sup>, Kabindra Adhikari <sup>d</sup>, Zicheng Wang <sup>a</sup>, Di Shi <sup>a</sup>, Xinxin Jin <sup>a,\*</sup>, Fengkui Qian <sup>a,\*</sup>

- a College of Land and Environment, Shenyang Agricultural University, Shenyang, Liaoning Province 110866, China
- b Key Laboratory of Ecosystem Network Observation and Modeling, Institute of Geographic Sciences and Natural Resources Research, CAS, Beijing 100101, China
- Institute of Bio- and Geosciences, Agrosphere (IBG-3), Forschungszentrum Jülich GmbH, Wilhelm-Johnen-Straβe, 52428 Jülich, Germany
- <sup>d</sup> USDA-ARS, Grassland, Soil and Water Research Laboratory, Temple, TX 76502, USA

#### ARTICLE INFO

## ABSTRACT

Keywords:
Soil organic carbon stocks
Climate change
Space-for-time substitution
Land use

Accurate assessment on temporal and spatial changes in soil organic carbon stocks (SOCS) is essential for evaluating the potential of soil carbon sequestration and formulating effective strategies to mitigate climate change. While most SOCS studies have focused on topsoil, there remains a lack of comprehensive understanding regarding the vertical distribution of SOCS within soil profiles. Furthermore, the key environmental variables influencing deep SOCS are still not fully comprehended. In this study, we employed an integrated approach combining equal-area spline function, boosted regression trees model (BRT), and the space-for-time substitution method to accurately model the three-dimensional distribution of SOCS in response to climate warming in Inner Mongolia, China. A total of 12 environmental variables (generated from climate, topography, biological, and soil property factor) and 208 soil profile data were selected to construct the model. The 10-fold cross-validation technique was employed to assess the predictive performance of the BRT model for soil organic carbon stocks (SOCS) at various depths, using four accuracy validation indicators: root mean square error (RMSE), mean absolute error (MAE), coefficient of determination (R<sup>2</sup>), and Lin's concordance correlation coefficient (LCCC). The results demonstrated the BRT model accurately predicted SOCS with higher LCCC and R<sup>2</sup> values, as well as lower RMSE and MAE values. The predicted map revealed higher SOCS concentration in the northeast and lower concentration in the western area, Grassland and forest land were found to store a majority of SOCS, with over 46 % located the topsoil depth of 30 cm. Furthermore, under different climate warming scenarios with temperature increase of 1.5 °C, 2 °C and 4 °C, there was a corresponding decreased in SOCS by 7 %, 9 % and 17 % respectively at a soil depth. Additionally, this study identified MAT and NDVI as primary environmental variables influencing the spatial distribution of three-dimensional scale SOCS. We believed that accurately predicting and mapping three-dimensional SOCS under different climate warming scenarios will contribute to the development of scientifically sound land management policies aimed at enhancing soil carbon sequestration in the region.

#### 1. Introduction

Soil constitutes the largest terrestrial carbon reservoir (1576 Pg), and even minor fluctuations in soil carbon can lead to significant alterations in atmospheric  $CO_2$  levels (Siegenthaler and Wenk, 1984; Lal, 2004) as well as global warming (Eswaran et al., 1993). As the primary constituent of land-based carbon reservoir, soil organic carbon (SOC) plays an important crucial role in regulating carbon cycle (Lal et al., 2004; Chen

et al., 2022). Understanding the response and adaptation of SOC to climate change is essential for predicting future climate change impacts (Berrang-Ford et al., 2011). Despite extensive research, several unresolved issues remain regarding the impact of warming on soil organic carbon stocks (SOCS) and its underlying mechanisms (Smith et al., 2008). Most studies focus on the topsoil SOCS while lacking sufficient understanding of SOC sensitive areas, depth intervals and key factors influencing changes in the deep SOCS (Lal et al., 2018; Chen et al.,

E-mail address: jinxinxin0218@syau.edu.cn (X. Jin).

<sup>\*</sup> Corresponding authors at: College of Land and Environment, Shenyang Agricultural University, No. 120 Dongling Road, Shenhe District, Shenyang, Liaoning Province 110866, China (X. Jin).

2022). Therefore, it is crucial to develop a reliable and efficient method for accurately predicting and mapping the spatial distribution of SOCS at three-dimensional scales amidst climate warming.

To effectively map soil attributes at different depths based on genetic soil horizons, it is recommended to standardize soil data to a uniform depth and utilize predictive models, particularly for datasets with inconsistent soil layer depth (e.g., those collected by Shahbazi et al., 2019). Currently, two primarily approaches are widely adopted: firstly, simulating the spatial distribution of SOCS at a depth of either 30 cm or 100 cm in accordance with IPCC guidelines (IPCC, 2006); secondly, employing the GlobalSoilMap specifications are for spatial predictions (Arrouays et al., 2014), supported rescue efforts (Arrouays et al., 2017). These well-established specifications have been successfully applied across various scales ranging from local regions to entire countries and even globally. Notable methods for modeling soil depth functions include statistical depth function (Zuo and Serfling, 2000), polynomial depth functions, (Jague et al., 2016), exponential depth function (Mishra et al., 2009), and equal-area spline function (ESF) (Bishop et al., 1999). Due to its high accuracy, smoothness, and stability in predicting the three-dimensional soil attributes' depth, ESF is extensively utilized in this context as highlight (Dharumarajan and Hegde, 2022). In France, Mulder et al. (2016) effectively modeled and predicted SOCS down to 1 m using the ESF combined with regression tree analysis. Adhikari et al. (2014) also adhered to the GlobalSoilMap specification while utilizing ESF along with Kriging method for predicting SOCS at five standard soil depths in Denmark.

The conventional approach to mapping the spatial distribution of SOCS involves calculating the mean SOCS value for each land use type or soil type and extrapolating it to all mapping units, but this method fails to capture the true spatial variability of SOCS (Khalil et al., 2013; Wang et al., 2020; Nguemezi et al., 2021). To obtain a representative average of SOCS levels, a large number of samples are typically required, which can be costly and time-consuming (Smith, 2004). Digital soil mapping (DSM) methods offer an effectively solution to address these challenges by leveraging limited sample data and comprehensive environmental analysis (Adhikari et al., 2019). DSM is based on the "scorpan" equation that posits soil formation and distribution as a result of a complex interactions between environmental variables known as soil formation factors such as climate, terrain, parent material, biology, and time (Minasny et al., 2013). Moreover, some environmental variables in the 'scorpan' equation can be adjusted through space-for-time substitution (STS) to predict future scenario under different climate or land use change (Blois et al., 2013). This approach has been widely used in other research as demonstrated by Adhikari et al. (2014) and Reyes Rojas et al.

Various DSM techniques are available for SOC mapping based on 'scorpan', including but not limited to support vector machines (Song et al., 2022), random forests (Grimm et al., 2008), stepwise multiple linear regression (Olaya-Abril et al., 2017), multivariate regression (Bhunia et al., 2019), and boosted regression trees (BRT) (Martin et al., 2011) among others. However, BRT model is widely acknowledged as an efficient and convenient approach that distinguishes itself from traditional tree models due to its integration of multiple simple tree models, enabling flexibly handling of linear, logical, exponential or general linear problems (Martin et al., 2011; Lamichhane et al., 2019).

In this study, we integrated ESF with the BRT and STS method to model the three-dimensional distribution of SOCS in response to climate warming in Inner Mongolia. Inner Mongolia, a long and narrow region extending from east to west in northern China, is considered an ecological barrier due to its geographical location and significant climate differences (Tian et al., 2011). The vegetation in Inner Mongolia is primarily distributed in the arid and semi-arid agro-pastoral ecotone, making its fragile ecosystem highly vulnerable to climate change impacts (Bai et al., 2004; Tian et al., 2011). Investigating the effects of climate warming on three-dimensional SOCS in Inner Mongolia will facilitate predictions of SOCS stability in this region and provide

scientific support for comprehending the changing trend of ecosystem carbon dynamics under global climate change (Zhang et al., 2022a; Zhang et al., 2022b). Therefore, Inner Mongolia serves as an optimal site for studying the impact of climate warming on SOCS. Our research objectives were: 1) developing a depth function model for simulating vertical distribution of SOCS; 2) identifying key environmental variables influencing spatial variation of the three-dimensional SOCS; 3) quantifying SOCS response under different land use patterns considering climate warming; and, 4) accurately depicting spatial distribution of multiple depths SOCS under various climate warming scenarios.

#### 2. Materials and methods

#### 2.1. Research region

This study was conducted in the Inner Mongolia, located in northern China (37°-53°N, 97.2°-126°E) (Fig. 1), encompassing an approximately area of  $1.1 \times 10^4$  km<sup>2</sup>. It shares borders with Russia and Mongolia to the north, spanning across the regions of Northeast China, North China, and Northwest China. Geographically demarcated by mountains ranges, the region exhibits a predominantly temperate continental monsoon climate (Zhang et al., 2022a; Zhang et al., 2022b). Weather patterns within the study area are characterized by a sudden temperature rise in spring followed by autumn, a short yet hot summer season, concentrated precipitation events, long and cold winter often accompanied by early frost occurrence (Bai et al., 2004). Most regions experience an annual sunshine duration exceeding 2700 h; however, the western region of Alashan Plateau receives over 3400 h of sunshine. Inner Mongolia is recognized as China's second-largest plateau due to its complex terrain and average altitude of approximately 1000 masl. Notably diverse topography exists within Inner Mongolia with plateau accounting for 53.4 %, mountains and hills comprising 37.3 %, plains and mudflat constituting for 8.5 %, while water bodies the remaining portion.

The soil type in Inner Mongolia exhibits significantly variation from east to west, resulting in a corresponding shift in the soil belt from northeast to southwest. In the eastern region is characterized by black soil, while the western region predominantly consists of dark brown, chernozem, chestnut, brown, black loessial, calcareous lime, sandy land and gray-brown desert soils (Bai et al., 2004; Chen et al., 2021). Among these soil zones, black soil stands out with its superior natural fertility, favorable structure and moisture condition for cultivation purposes. Consequently, it is highly suitable for agricultural development. The chernozem's inherent fertility makes it an excellent choice for crop cultivation as well as forestry and animal husbandry activities. Grassland covers the largest proportion of land use types at 46 %, followed by unused land (28 %), forest land (14 %), arable land (10 %), while construction and wetland each account for only 1 %.

#### 2.2. Soil profile data

The soil dataset was digitized from the book "Soil series of China, Inner Mongolia Volume" published by National Science and Technology Basic Resources Survey Program of China (2008FY110600). This collaborative effort between Shenyang Agricultural University and Nanjing Institute of Soil Research, Chinese Academy of Sciences resulted in its officially published in 2020. Fieldwork conducted between 2017 and 2018 collected soil profile information, which was subsequently analyzed at Shenyang Agricultural University in 2018. We meticulously digitized all the soil profile data from the aforementioned book to create an up-to-date soil dataset for Inner Mongolia, China. The dataset includes comprehensive described of each soil profile along with analyzed results for soil organic carbon content using the dry combustion method (Matejovic, 1993) based on a total of 809 soil samples. Additionally bulk density was determined through oven-dry methods (Erbach, 1987), and gravel content information is also provided.

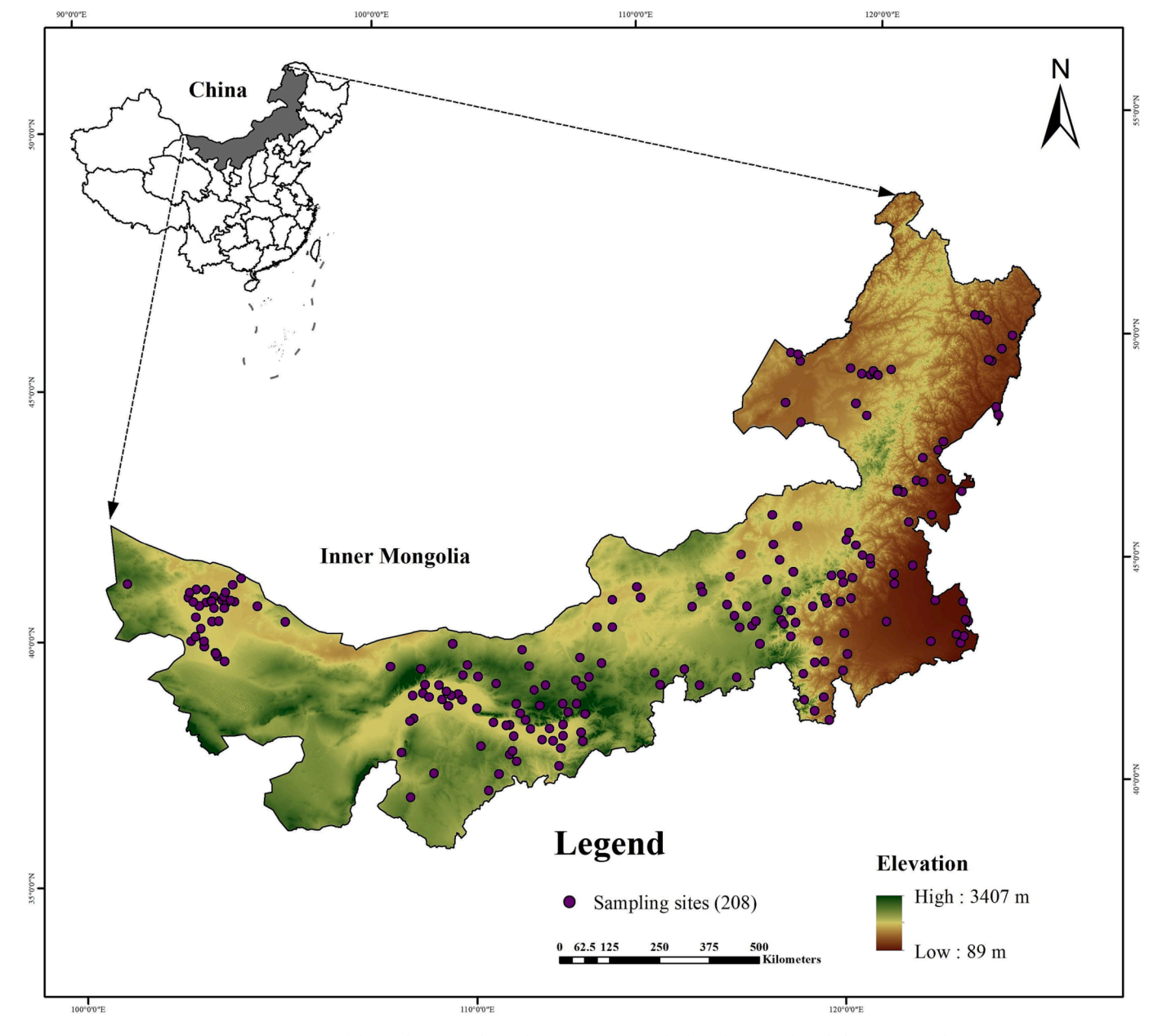


Fig. 1. Location of the study area and sampling point map overlaid on the 90-m digital elevation model.

## 2.3. Calculation of SOCS

The objective of this study was to investigate the spatial variation of three-dimensional SOCS under different climate warming scenarios. We employed the Batjes (1996) formula to calculate SOCS in each special soil layer throughout the entire profile (Eq. (1):

$$SOCS = \sum_{i=1}^{k} SOC_{content} = \sum_{i=1}^{k} SOC_{concentration} \times BD_{i} \times D_{i} \times (1 - S_{i})$$
 (1)

where *SOCS* represents the SOC density (kg m $^{-2}$ ); *SOC*<sub>content</sub>, denotes the SOC content (kg m $^{-2}$ ) of each k layer; SOC<sub>concentration</sub> refers to the SOC concentration (g kg $^{-1}$ ); BD stands for the bulk density (g cm $^{-3}$ ); D represents the thickness of soil layer (m); S indicated the volume fraction of fragments > 2 mm (%); and i refers to a specific layer within the soil profile.

## 2.4. Environmental data

In this study, a total of 12 environmental variables (including soil, topographic, climatic, and biological variables) were selected to accurately predict the three-dimensional SOCS response to climate warming in Inner Mongolia. Due to the diverse sources of data on environmental biological variables, all data layers were reprojected and resampled to Albers Conical Equal Area projection at a 90 m spatial resolution using ArcGIS 10.2 (ESRI Inc., USA). Subsequent analysis and modeling of the data were conducted using R software (R Development Core Team, 2013).

#### 2.4.1. Climatic variables

Climate variables, such as temperature and precipitation, exert a substantial impact influence on the accumulation and decomposition of SOC (Gibson et al., 2021). The climatic variables utilized in this study encompassed mean annual temperature (MAT) and mean annual precipitation (MAP), obtained from the Geospatial Data Cloud site of the

Chinese Academy of Sciences (http://www.gscloud.cn), MAT and MAP were derived from daily observation collected by 2400 meteorological stations nationwide, which were subsequently interpolated using thin pate smooth splines with ANUSPLIN software (McKenney et al., 2006). Initially available at a spatial resolution of 1 km  $\times$  1 km, the downloaded data was resampled to a higher resolution of 90 m  $\times$  90 m. Furthermore, to address the potential impact of climate warming on variation in SOCS, we incorporated scenarios representing an increase in MAT by 1.5 °C, 2 °C and 4 °C into the MAT layer to derive corresponding variables for different climate warming scenarios (Lan et al., 2021). The Paris Climate Agreement establishes a global temperature rise limit of 1.5 °C, as indicated by King and Karoly (2017). Once this threshold is surpasses, it will have significantly implications for human daily life and production, leading to more frequent occurrences of extreme high temperature, heavy rainfall, drought, and wildfire (Aerenson et al., 2018). If the global average temperature exceeds a 2 °C increase from pre-industrial levels, it will exacerbate the adverse impacts of climate change on both economic growth and environmental quality (King and Karoly, 2017). A rise to or above 4°C would not only result in the extinction of numerous endangered species but also the likelihood of wide-range and impact extreme weather events (Adams et al., 2013). Therefore, this study has considered these three distinct warming scenarios to model and predict SOCS in in Inner Mongolia.

#### 2.4.2. Topographic variables

Six topographic variables, namely slope gradient (SG), elevation (ELE), slope aspect (SA), catchment area (CA), profile curvature (PG), and topographic wetness index (TWI), were derived from a digital elevation model (DEM) obtained from the Geospatial Data Cloud site of the Chinese Academy of Sciences (http://www.gscloud.cn). These topographic variables are commonly utilized in predicting soil properties, such as SOCS, by indicating the redistribution of surface materials, water, and energy fluxes within a given landscape. (Román-Sánchez et al., 2018; Blackburn et al., 2022). Overall, ELE influences the formation and distribution of soil properties, enzymes, and microorganisms, thereby affecting SOC levels and leading to feedback on SOCS change (Tsozué et al., 2019). SG and SA impact SOCS through factors such as soil thickness, vegetation coverage, organic matter input, and human disturbance (Wang et al., 2020). PC exerts an influence on flow velocity and drainage processes that subsequently affect erosion and deposition dynamics (Blackburn et al., 2022). TWI, and CA comprehensively consider the influence of terrain characteristics on potential soil moisture retention and distribution (Román-Sánchez et al., 2018). ELE. SG, SA, and PC were derived from DEM data in ArcGIS 10.2, while CA and TWI were calculated using SAGA GIS (Conrad et al., 2015).

#### 2.4.3. Biological variables

The Normalized Difference Vegetation Index (NDVI) plays a crucial role in detecting vegetation growth and coverage, as the prediction of SOC levels (Adhikari et al., 2019; Shafizadeh-Moghadam et al., 2022). Jobbágy and Jackson (2000) established a robust correlation between the distribution pattern of SOC and NDVI. Moreover, due to its capacity to indicate vegetation productivity and biomass, NDVI is extensively employed for predicting SOCS. The 2018 NDVI data was acquired from the Geospatial Data Cloud site of the Chinese Academy of Sciences (htt ps://www.gscloud.cn) and resampled to a 90-m grid.

#### 2.4.4. Soil variables

The study utilized soil texture data, encompassing percentages of sand, silt and clay content, as predictors for SOCS. Soil texture exerts a well-established influence on diverse properties and processes such as permeability, moisture retention, aggregation and fertility (Dharumarajan and Hegde, 2022). The soil texture data used in this study were acquired from the Resource and Environmental Science and Data Center of the Chinese Academy of Sciences (https://www.resdc.cn). This dataset was generated by integrating a 1:1 million scale soil survey map

with soil profile data obtained from the second national soil survey, these data were converted into a raster format with a resolution of 1 km  $\times$  1 km.

#### 2.5. Prediction models

This study used equal-area spline function, boosted regression tree (BRT), and Space-for-time substitution method to predict SOCS at different soil depths in response to climate warming. The specific flowchart of the methodology was shown in Fig. 2.

#### 2.5.1. Equal-area spline function

The Malone et al. (2009) equal-area spline function, which is based on Bishop et al.'s (1999) quadratic spline function, was employed using SplineTool Version2 (ASRIS, 2011) to model SOCS profile measurements. This tool enables the modeling of a continuous depth function based on discrete SOCS measurements obtained from non-overlapping soil layers or horizons. The modeled values can be aggregated into specific intervals representing different soil depth. It is assumed that the measurement from each soil layer i represents the mean value, accounting for any potential measurement error. Mathematically, the measured can be represented as follows:

$$y_i = \overline{f_i} + e_i \tag{2}$$

where  $y_i$  represents the actual mean value of soil attribute within the given interval  $(x_{i-1}, x_i)$ ;  $\bar{f}$  represents the average measurement value;  $e_i$  represents the measurement error and independent; i represents the soil depth layer. The underlying assumption posits a smooth variation of soil attribute values with depth. The function f(x) denotes a spline obtained through minimizing Di:

$$D_{i} = \frac{1}{n} \sum_{i=1}^{n} (y_{i} - \overline{f_{i}}) + \lambda \int_{x_{0}}^{x_{n}} \left[ f^{m}(x)^{2} \right] dx$$
 (3)

The first term of equation represents the data fitting, while the second term quantifies the smoothness of function f(x) through its first derivative f'(x). The parameter  $\lambda$  determines the trade-off between fitting and roughness, and this study tested five different values for  $\lambda$  (0.0001, 0.001, 0.01, 0.1, and 1) to identify the optimal fit. Among these values, a  $\lambda = 0.1$  yielded the lowest root mean square error.

#### 2.5.2. Boosted regression trees

The BRT model was utilized to simulate the spatial variation of SOCS and assess the relative importance (RI%) of climate, terrain, biological and soil variables on SOCS. The BRT model combines regression tree algorithm and boosting method, offering several advantages such as adaptability to complex nonlinear relationships, automatic handling of variable interactions, and improved stability and accuracy (Elith et al., 2008; Wang et al., 2020). The BRT model requires user to specify four parameters: learning rate (LR), tree complexity (TC), bag fraction (BF) and tree number (NT) (Elith et al., 2008). LR represents the influence of an individual tree on the final model's performance (Wang et al., 2020). TC reflects the intricate and multifaceted nature of each decision tree (Martin et al., 2011). BF index indicates the degree of randomness in the data set selection levels of randomness (Wang et al., 2022). Determining NT determination can be achieved by combination LR and TC (Lamichhane et al., 2019). To identify optimal parameters, we tested various combinations within ranges for LR (0.25-0.0025), TC (8-12), BF (0.55–0.75) and NT (800–2500). Ultimately, we determined the optimal values for LR, TC, BF, and NT were respectively found to be 0.025, 12,  $0.75,\, and\, 1500$  with minimal error rates.

#### 2.5.3. Space-for-time substitution method

The formation and development of soils are influenced by a range of environmental variables. These factors, collectively referred to as "scorpan" factors of soil formation (McBratney et al., 2003; Adhikari

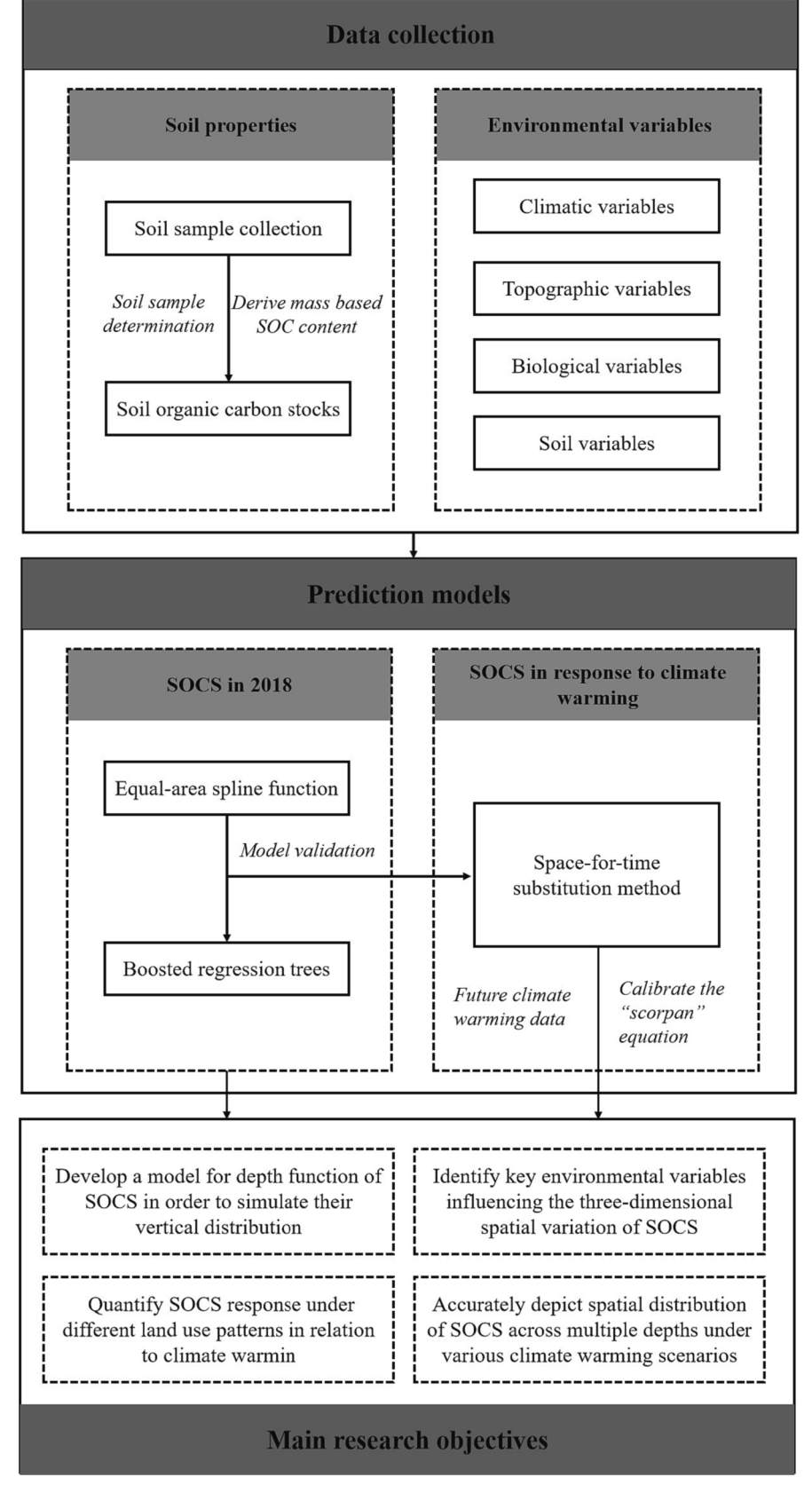


Fig. 2. Flowchart of the methodology.

et al., 2019), play crucial roles in the process of soil development. The spatial-temporal effects of these factors can be quantified using a STS method (Adhikari et al., 2019), where one factor is manipulated while keeping other factors constant. For instance, to investigate the impact of temperature on the distribution of SOCS, various temperature scenarios can be tested and their effects on SOCS can be measured. This approach has effectively assessed the spatial variation of SOCS across diverse land use and climate change scenarios in Brazil, Australia, Chile, United States, and China (Strey et al., 2016; Adhikari et al., 2019; Gomes et al., 2019; Wang et al., 2022). However, despite its the validity of this method cannot be tested without verification data for future scenario and uncertainties may exist (Strey et al., 2016; Gray and Bishop, 2016; Reyes Rojas et al., 2018). To investigate the response of the SOCS to future climate warming scenario in Inner Mongolia, this study utilized the profile data from 2018 along with 12 environmental variables as predictors. It was assumed that environmental factors such as parent material or terrain would remain relatively stable over a given period in the future. The STS method was employed to capture the spatiotemporal dynamics of SOCS in response to anticipated temperature fluctuations.

#### 2.6. Accuracy evaluation

The predictive performance of BRT model was evaluated using a 10-fold cross-validation technique, which involved calibrating and testing of each sample data point. Four validation indices, namely MAE, RMSE, coefficient of determination (R<sup>2</sup>), and Lin's consistency correlation coefficient (LCCC) (Lin, 1989) were utilized to assess the model's performance (Eq. 4–7).

$$MAE = \frac{1}{n} \sum_{i=1}^{n} |a_i - b_i|$$
 (4)

$$RMSE = \sqrt{\frac{1}{n} \sum_{i=1}^{n} (a_i - b_i)^2}$$
 (5)

$$R^{2} = \frac{\sum_{i=1}^{n} (a_{i} - \overline{b}_{i})^{2}}{\sum_{i=1}^{n} (b_{i} - \overline{b}_{i})^{2}}$$
 (6)

$$LCCC = \frac{2r\partial_a\partial_b}{\partial_a^2 + \partial_b^2 + (\overline{a} + \overline{b})^2}$$
 (7)

where  $a_i$  and  $b_b$  represent predicted values and measured values;  $\overline{a}$ , and  $\overline{b}$  is the mean of predicted values and measured values; n represents the number of sampling points; r denotes the correlation coefficient between

measured and predicted values;  $\partial_a$  and  $\partial_b$  are variances of predicted and measured values.

#### 3. Results

#### 3.1. Exploratory data analysis

The continuous depth function of SOCS was modeled using an ESF. Table 1 presents summary statistics for aggregated SOCS at different depths (0–5 cm, 5–15 cm, 15–30 cm, 30–60 cm and 60–100 cm), along with the corresponding statistics for predictors for SOCS. In the topsoil (0–5 cm), the range of SOCS varied from 0.03 to 4.13 kg m $^{-2}$ , while in the subsoil (60–100 cm), it ranged from 0.07 to 14.71 kg m $^{-2}$ . The mean value of SOCS increased gradually with depth, reaching its peak at a depth of 30–60 cm and exceeding that of the surface layer by more than threefold. All soil depths exhibited positively skewed distributions in terms of their SOCS values, with the highest skew value being observed at a depth of 15–30 cm.

The correlation coefficients between SOCS and environmental variables revealed significantly positive correlations with SG, MAP, NDVI, clay, and negative correlations with CA, TWI, and MAT at all soil depth levels (Table 2). Among these variables, MAT exhibited the stronger correlation with SOCS, followed by NDVI and MAP. We assessed multicollinearity among these variables by calculating the variance inflation factor (VIF) while considering their intercorrelations. The results indicated that there was no issue of multicollinearity in the predicting SOCS in 2018 as evidenced by each environmental variable's VIF.

#### 3.2. Model performance

To enhance prediction robustness, the BRT model was executed 100 times and the average values were utilized as the final forecasted outcome. The BRT model demonstrated satisfactory predictive performance across all soil depths; however, a decreasing trend in accuracy was observed with increasing depth. Optimal performance was observed at 5–15 cm and 15–30 cm, while suboptimal performance occurred at greater depths (60–100 cm) (Table 3), as evidenced by higher R<sup>2</sup> and LCCC scores and lower MAE and RMSE scores.

### 3.3. Relative importance of environmental variables

The BRT model was iterated 100 times and the average RI of each environmental variable was calculated. To ensure comparability across different depth layers, the RI values were then standardized to scale to 100 %. Across all depth layers, NDVI, MAT and MAP were the primary

 Table 1

 Descriptive statistics of soil organic carbon stocks (SOCS) at different depths and environmental variables based on 208 sampling points.

Property	Unit	Min.	Max.	Mean	Skewness	Kurtosis
SOCS <sub>0-5</sub>	${\rm kg}~{\rm m}^{-2}$	0.03	4.13	0.90	1.45	3.18
SOCS <sub>5-15</sub>	${ m kg}~{ m m}^{-2}$	0.11	10.1	1.79	1.95	6.48
SOCS <sub>15-30</sub>	${ m kg}~{ m m}^{-2}$	0.15	17.9	2.34	2.86	16.6
SOCS <sub>30-60</sub>	$ m kg~m^{-2}$	0.21	14.0	3.35	1.42	2.12
SOCS <sub>60-100</sub>	${ m kg}~{ m m}^{-2}$	0.07	14.7	3.01	1.63	3.22
ELE	m	126.7	1945.5	938.7	-0.16	-0.27
SG	Degree	0.01	6.80	0.81	2.46	8.86
SA	Degree	1.10	357.3	158.1	0.37	-1.20
CA	$\mathrm{m}^2~\mathrm{m}^{-1}$	7,330,910	2,306,450,000	723,194,273	0.54	-0.76
PC	Index	-0.02	0.02	0.00	0.40	16.6
TWI	Index	8.38	15.02	12.4	-0.13	-0.86
MAP	Celsius degree	39.9	606.3	297.9	-0.23	-0.85
MAT	mm	-2.07	10.7	5.13	-0.19	-1.01
NDVI	Index	0.06	0.86	0.48	-0.27	-1.17
Clay	Percentage	4.00	33.0	17.3	-0.14	-0.68
Silt	Percentage	7.00	49.0	27.0	-0.07	0.59
Sand	Percentage	24.0	85.0	55.5	0.05	-0.39

Note: ELE, elevation; SG, slope gradient; SA, slope aspect; CA, catchment area; PC, profile curvature; TWI, topographic wetness index; MAP, mean annual precipitation; MAT, mean annual temperature; NDVI, Normalized Difference Vegetation Index.

Property	$SOCS_{0-5}$	$SOCS_{5-15}$	$SOCS_{15-30}$	$SOCS_{30-60}$	$SOCS_{60-100}$	ELE	SG	SA	CA	PC	TWI	MAP	MAT	NDVI	Clay	Silt
SOCS <sub>5-15</sub>	0.95															
$SOCS_{15-30}$	0.75**	0.88**														
$SOCS_{30-60}$	0.67**	0.67**	0.73**													
$SOCS_{60-100}$	0.43**	0.43**	0.45**	0.72**												
ELE	-0.22**	-0.23**	-0.18*	-0.04	0.03											
SG	0.24**	0.22**	0.21**	0.18**	0.19**	0.11										
SA	90.0	0.07	90.0	0.03	80.0	0.02	0.03									
CA	-0.27**	-0.28**	-0.30**	-0.24**	-0.15*	-0.29**	-0.55**	0.03								
PC	-0.10	-0.12	-0.14*	-0.12	-0.07	0.20**	0.27**	90.0	-0.05							
TWI	-0.40**	-0.39**	-0.39**	-0.35**	-0.26**	-0.15*	-0.76**	-0.05	0.77	-0.04						
MAP	0.57**	0.50**	0.55	0.48**	0.40**	-0.26**	0.43**	0.11	-0.43**	-0.05	-0.63**					
MAT	-0.63**	-0.63**	-0.59**	-0.51**	-0.35**	0.19**	-0.38**	-0.12	0.39	0.00	0.54**	-0.62**				
NDVI	0.62**	0.60**	0.53**	0.43**	0.37**	-0.46**	0.30**	0.14*	-0.16*	-0.05	-0.39**	0.77**	-0.60**			
Clay	0.42**	0.40**	0.33**	0.28	0.16*	-0.14*	0.23**	-0.05	-0.22**	0.09	-0.33**	0.41**	-0.37**	0.47**		
Silt	0.03	0.03	0.00	-0.04	-0.09	0.11	-0.01	-0.03	0.03	0.16*	0.01	-0.04	80.0	0.01	0.62**	
Sand	-0.23**	-0.22**	-0.16*	-0.12	-0.02	0.00	-0.11	0.05	0.09	-0.14*	0.16*	-0.18*	0.14	-0.24**	-0.88**	-0.92**

Note: ELE, elevation; SG, slope gradient; SA, slope aspect; CA, catchment area; PC, profile curvature; TWI, topographic wetness index; MAP, mean annual precipitation; MAT, mean annual temperature; NDVI, Normalized Difference Vegetation Index

**Table 3**Summary statistics of soil organic carbon stocks prediction performance of boosted regression tree models in 2018.

Depth (cm)	MAE	RMSE	$R^2$	LCCC
0–5	0.21	0.27	66.13	0.76
5–15	0.20	0.25	67.62	0.79
15-30	0.20	0.25	67.54	0.78
30-60	0.21	0.28	51.56	0.68
60-100	0.29	0.37	32.59	0.40

**Note:** MAE, mean absolute error; RMSE; RMSE, root mean squared error; R<sup>2</sup>, coefficient of Determination; LCCC, Lin's concordance correlation coefficient.

drivers of spatial variability in SOCS, followed by topographic variables, with soil variables exhibited the least RI (Fig. 3). At depths of 0–5 cm and 5–15 cm, MAT and NDVI were the most influential variables on SOCS spatial variation, accounting for over 30 % of total RI. Climatic variables such as MAT or MAP had a more pronounced impact at surface layers compared to deeper layer (60–100 cm). Similarly, topographic variable demonstrated moderate significance while soil properties including sand, silt, clay content showed relatively low RI across all soil horizons

#### 3.4. Spatial variation of SOCS

The spatial variation of SOCS at five soil depths was depicted in Fig. 4 for three warming scenarios (1.5 °C, 2 °C, and 4 °C) in 2018. Under these warming scenarios, the spatial distribution characteristics of SOCS exhibited a consistent pattern with a gradual decrease from northeast to southwest. The majority of SOCS was found to be stored in 30-60 cm layer, followed by 15-30 cm, 60-100 cm, 5-15 cm and 0-5 cm layers (Fig. 4). Under three distinct scenarios (1.5 °C, 2.0 °C and 4 °C), the mean SOCS at a depth of 30-60 cm in 2018 were 2.83  $\pm$  1.27 kg m<sup>-2</sup>  $2.64 \pm 1.21 \text{ kg m}^{-2}$ ,  $2.58 \pm 1.18 \text{ kg m}^{-2}$ , and  $2.39 \pm 1.06 \text{ kg m}^{-2}$ . Furthermore, we computed the sum of SOCS for 0-30 cm and 0-100 cm to determine the overall in the top 30 cm and up to a depth 1 m under various climate warming scenarios (Fig. 5). With the temperature increasing by 4°C from the base period (2018), SOCS gradually decreased in the topsoil (0–30 cm) from 4.47  $\pm$  2.79 kg m $^{-2}$  to 3.39  $\pm$ 2.24 kg  $m^{-2}$  and in the whole profile (0–100 cm) from 9.67  $\pm$  4.62 kg  $m^{-2}$  to 7.99  $\pm$  3.84 kg  $m^{-2}$ .

Additionally, we conducted calculations on the SOCS at various soil depths in response to climate warming (Table 4). It was observed that Inner Mongolia exhibited the highest SOCS at a depth of 30-60 cm. Under three distinct scenarios (1.5 °C, 2.0 °C and 4 °C), the SOCS at a depth of 30-60 cm in 2018 were 3061 Tg, 3002 Tg, 2778 Tg, and 3283 Tg. Within the entire 1 m-deep soil layer, the majority of SOCS was predominantly stored within depths ranging from 0 to 30 cm; specifically accounting for approximately 46 %, 45 %, 45 %, and 42 % under initial conditions in 2018 and scenarios of temperature increase by 15°C, 2 °C, and 4 °C respectively. The SOCS responses to various climate warming scenarios at two depth levels (0-30 cm and 0-100 cm) under different land use types were presented in Table 5. Grasslands emerged as the primary storage site for SOCS, accounting for approximately 50 % of the total SOCS across all three climate warming scenarios. Forest lands, arable lands, unused lands, construction lands followed in descending order, while wetlands exhibited the lowest amount of stored SOCS. Furthermore, the amount SOCS present in the topsoil (0–30 cm) was equivalent to approximately 46 % of that detected at a soil depth of 1 m. To investigate variations in SOCS with respect to land use and depth, we presented a sliced distribution along longitude 121°E in response to climate warming (Fig. 6). We observed a gradual decreased in SOCS with increasing temperature towards lower latitude. The majority of stored SOCS was found in grassland and forest land, whereas changes in arable land and construction land were negligible.

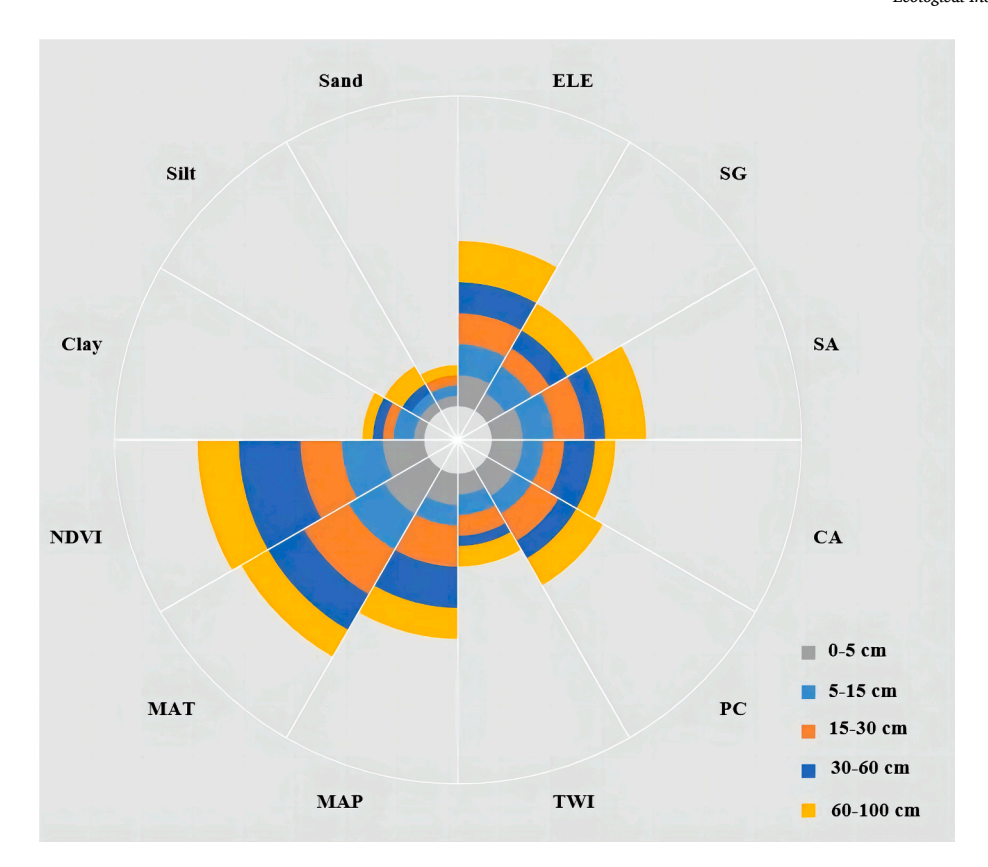


Fig. 3. Relative importance of environmental variables based on 100 iterations of the BRT model in 2018. ELE, elevation; SG, slope gradient; SA, slope aspect; CA, catchment area; TWI, topographic wetness index; PC, profile curvature; MAP, mean annual precipitation; MAT, mean annual temperature.

#### 4. Discussion

### 4.1. Controls of SOCS

The BRT model identified NDVI, MAT and MAP as primary environmental variables that exert a significant influence on the spatial variability of SOCS, followed by topographic and soil property variables (Fig. 3). In areas characterized by complex and dynamic terrain, topographic variables were found to be reliable predictors of SOCS (Yang et al., 2016). The terrain indirectly affects the soil though the material and energy redistribution, as demonstrated in studies conducted by Román-Sánchez et al., (2018) and Gomes et al. (2019). This study confirmed previous findings that ELE was the dominant variable affecting spatial variability in SOCS (Yang et al., 2016; Blackburn et al., 2022). Tsui et al. (2013) have previously shown ELE to be a highly effective predictor of SOCS in Yangmingshan National Park in Taiwan, China. We observed that SA exhibited greater relative significance than ELE in the layer of 60-100 cm depth. The diminishing influence of environmental variables on SOCS spatial variability with soil depth can be attributed to inherent physical and chemical properties of the soil (Yang et al., 2016). SA indirectly affects the physical and chemical properties of soil in mountainous regions through its regulation of lighting conditions, precipitation, and temperature (Gomes et al., 2019). Rezaei and Gilkes (2005) conducted that the SOC varied with depths and slope direction, showing a significant increase in deep SOC on shady slopes.

Previous studies have demonstrated that MAT and MAP were the primary climatic variables influencing the spatial variability of SOCS (Fang et al., 2005; Nguemezi et al., 2021). Our study revealed that MAT exhibited the highest RI among all environmental variables at topsoil (0–5 cm and 5–15 cm), with its significance gradually diminishing with increasing depth. This finding is consistent with previous research findings by Zhou et al. (2019) and Jobbágy and Jackson (2000). Wang

et al. (2004) observed a pronounced peak in the correlation between SOC and MAT in the, topsoil, while its influence gradually decreased with depth. Using the NSCD and WISE soil database, Jobbágy and Jackson (2000) found a positive correlation between total SOC content, precipitation, and clay content, while observing a negative correlation with temperature. The significance of controlling factors varied depending on depth: climatic variables played a dominant role in shallow layers, whereas clay content was identified as the primary determinant in deeper layers.

The NDVI was identified as a crucial variable influencing the spatial variation of SOCS, consistent with previous findings by Bangroo et al. (2020) and Shafizadeh-Moghadam et al. (2022). This study further confirmed the significance of NDVI, which exhibited the second highest RI among all variables at depths of 0-5 cm and 5-15 cm, and emerged as the most influential environmental variable below a depth layer of 5-15 cm (Fig. 3). In the Garhwal Himalaya, India, Kumar et al. (2022) conducted an assessment of SOCS across a gradient of chir pine forests and established NDVI as a reliable predictor. Mondal et al. (2017) recognized NDVI as the primary environmental variable governing SOC levels and observed a strong correlation between topsoil SOC distribution patterns and NDVI values. Surprisingly, despite reflecting vegetation productivity and biomass, NDVI exhibited higher RI values at all depths (Fig. 3). In Inner Mongolia, grasslands and forests account for approximately 75 % of the total area, significant amounts of humic organic matter are deposited into soils through dead stems/branches, fallen leaves, and roots. Furthermore, low winter temperature may impede organic matter decomposition leading to SOC accumulation. Interestingly though soil data revealed lower RI values across all depth levels contradicting. Jobbágy and Jackson (2000) proposition that deep soil SOCS was primarily determined by the clay content; instead minimal RI values associated with clay content at all depth. We postulate that the impact of clay content on SOCS may have been mitigated by topographic and climatic variables. Table 2 further supports this hypothesis by

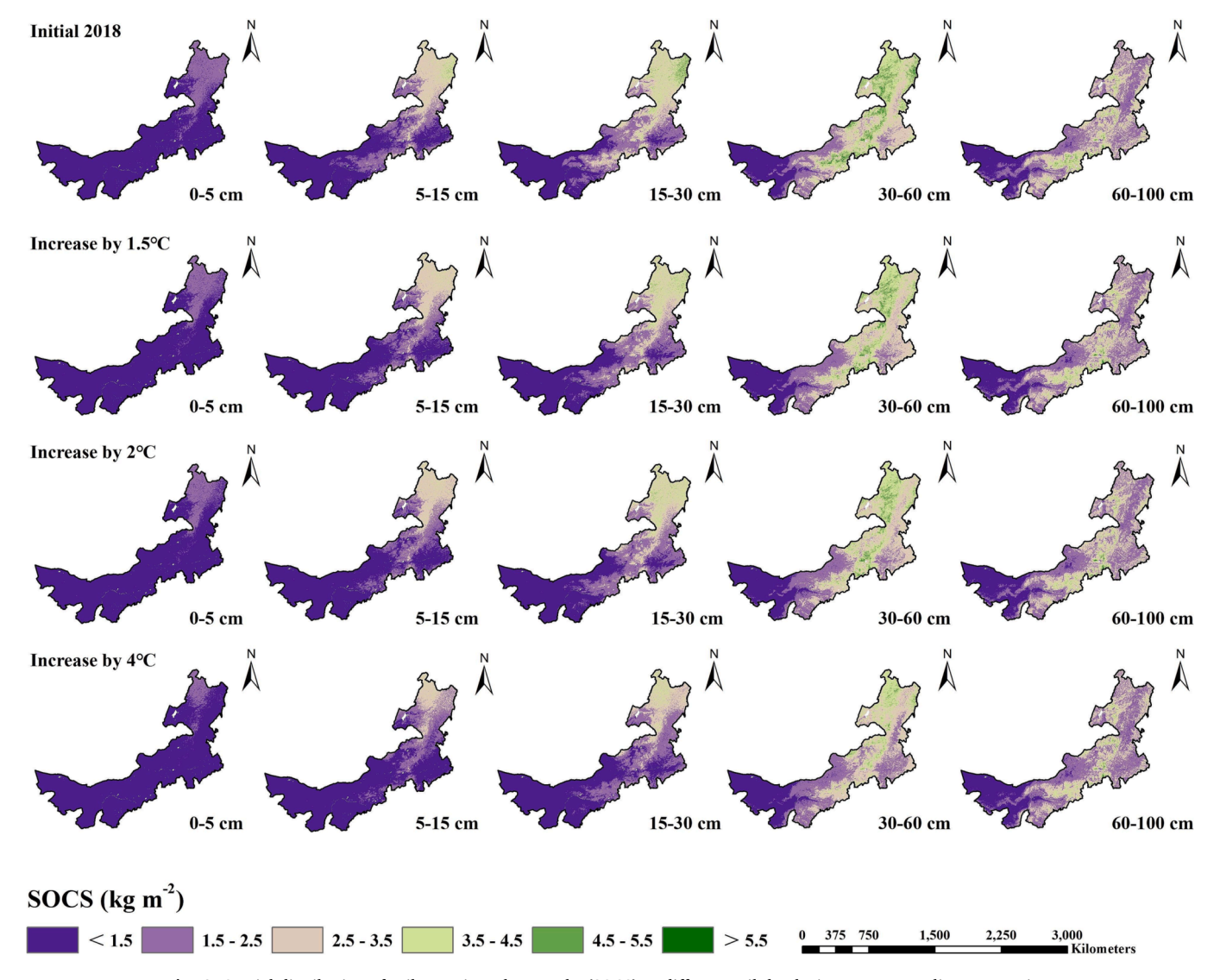


Fig. 4. Spatial distribution of soil organic carbon stocks (SOCS) at different soil depths in response to climate warming.

demonstrating significant correlations between clay content and ELE, SG, CA, TWI, MAP, and MAT.

#### 4.2. Response of SOCS to climate warming

The spatial distribution trend of SOCS across different soil depths exhibited similar patterns under different warming scenarios (Fig. 4). The highest concentration of SOCS was predominantly observed in the forests and grasslands located in the northeastern region, characterized by a primarily humid and semi-humid climate. Additionally, Bai et al. (2004) suggested that the warm summers, sufficient rainfall, and cold, long winters in Inner Mongolia promoted the accumulation of soil organic matter. The lower SOCS was primarily distributed in the western region, which was predominantly a temperate desert arid area characterized with sparse shrub and semi-shrub vegetation. Our research findings indicated that the spatiotemporal variation of SOCS in Inner Mongolia was primarily influenced by a combination of climatic and biological factors, with temperature exerting a greater impact on its spatial pattern (Fig. 6). This finding aligned with previous research conducted by Smith et al. (2008) and Gibson et al. (2021). In permafrost regions of the Northern Hemisphere, Wu et al. (2022) employed machine learning techniques to estimate SOC distribution at 3 m depth and identified that MAT and NDVI as primary factors controlling its spatial distribution in northern and third polar permafrost regions.

To gain a deeper understanding of the impact of climate warming on the spatial distribution of three-dimensional SOCS, we present a cross-sectional analysis of soil at a depth of 1 m along longitude  $121^{\circ}E$  (Fig. 6). Our observations reveal a gradual decline in SOCS as MAT increases. However, under different climate warming scenarios, there is a progressive reduction in SOCS, with the maximum decrease occurring at 4 °C. The acceleration of organic matter decomposition due to climate warming is expected to result in decreased soil carbon content, which aligns with previous findings by Smith et al, (2008). This phenomenon is further supported by our study. Jones et al. (2005) proposed that the increase in decomposition rate caused by climate warming may surpass net primary productivity, potentially leading to a decline in SOC levels. Similarly, Zhao et al. (2021) found that SOC loss on the Chinese Loess Plateau was largely driven by temperature increases.

Additionally, we computed the SOCS of various land use patterns under different climate warming scenarios (Table 5). In Inner Mongolia, SOCS was primarily sequestered in grassland and forested areas across varying degrees of climate warming. With a temperature increased of 1.5 °C, 2 °C and 4 °C, SOCS in the topsoil (0–30 cm) decreased by 10 %, 13 % and 24 %; while those in the subsoil (0–100 cm) declined by 7 %, 9 % and 17 %. Among all the land use types, grassland exhibited the most significant reduction in SOCS, accounting for approximately 50 % of the total SOCS in both depth layers (Table 5). Climate warming not only affected litter input, but also had a substantial impact on SOC

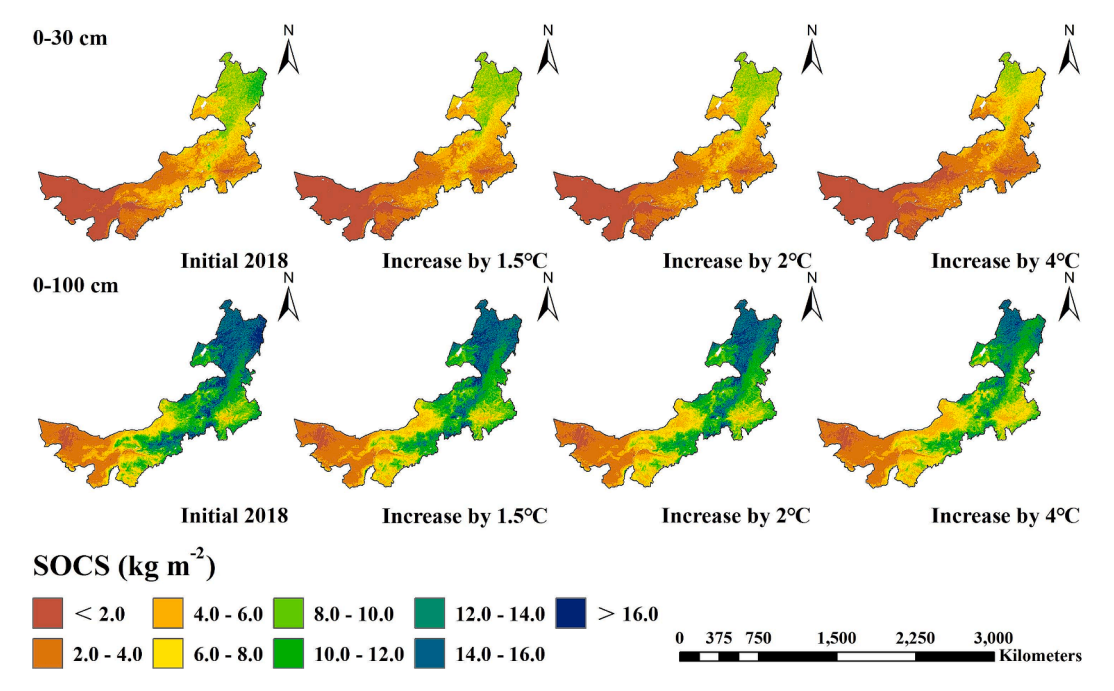


Fig. 5. Spatial distribution of soil organic carbon stocks (SOCS) at 0-30 and 0-100 cm in response to climate warming.

**Table 4**Summary statistics of soil organic carbon stocks at different soil depths in response to climate warming.

Soil layers (cm)	Initial 2018 (Tg)	Increase by 1.5℃ (Tg)	Increase by 2°C (Tg)	Increase by 4°C (Tg)
0-5	965.95	864.64	835.59	716.47
5-15	1855.89	1677.45	1625.6	1415.93
15-30	2343.57	2118.02	2050.61	1792.35
30-60	3283.77	3061.15	3002.05	2778.06
60-100	2728.64	2648.53	2626	2553.03
Total	11177.82	10369.79	10139.85	9255.84

decomposition rate (Fang et al., 2005; Shafizadeh-Moghadam et al., 2022). Zhao et al. (2021) discovered that climate warming accelerated soil carbon decomposition and released it into the atmosphere, exacerbating global warming. The increase in soil microbial activity and biomass caused by climate warming played a crucial role in accelerating SOC decomposition (Jones et al., 2005; Adhikari et al., 2019). Furthermore, climate warming not only significantly influenced SOC, but also altered its composition with increasing temperature (Gibson et al., 2021). Jobbágy and Jackson (2000) observed an increased in the active carbon pool while the total SOC remained relatively stable, however, with continuous climate warming trends suggest a decline.

#### 4.3. Research limitations

A combination of BRT model, ESF and STS method can offer

relatively accurate predictions of SOCS in response to climate warming at three-dimensional scale. However, this study still had some evident uncertainties. Firstly, the soil data was obtained from the digitized book of Soil series of China, which might not fully reflect the actual situation in the region due to the differences in research objectives and could lead to prediction errors; Secondly, environmental variables were downloaded from various platforms with varying resolutions and formats, potentially resulting in information loss during resampling to a unified resolution and format; Thirdly, this study solely employed the ESF for simulating SOCS variation at different depth; however, the spatial heterogeneity of SOCS at vertical depth was intricate. Therefore, simulation outcomes at certain sampling points may significantly deviate from actual results and lead to prediction errors; Fourthly, this study only considered climate warming scenario, of 1.5 °C, 2 °C and 4 °C under climate change, while assuming that other environmental variables remain constant. However, it was worth nothing that potential impact of warming on precipitation was not taken into account in our analysis, which might result in deviation between simulation results and actual observations; Fifthly, the influence of environmental variables on SOCS diminished as soil depth increased, with the spatial variation of deep SOCS being predominantly shape physical and chemical characteristics of the soil. It should be noted that this study utilized environmental variables to simulate deep SOCS, which might deviate from actual conditions.

**Table 5**Summary statistics of soil organic carbon stocks under different land use patterns in response to climate warming.

Land use patterns	Area (km²)	Initial 2018	(Tg)	Increase by	Increase by 1.5°C (Tg)		Increase by 2°C (Tg)		Increase by 4°C (Tg)	
		0-30 cm	0–100 cm	0-30 cm	0–100 cm	0-30 cm	0–100 cm	0-30 cm	0–100 cm	
Arable land	113,922	626.16	1355.12	547.90	1228.43	527.14	1194.56	452.92	1078.75	
Forest land	165,060	1295.84	2336.22	1218.27	2224.36	1187.51	2182.54	1047.32	2000.06	
Grassland	532,190	2550.44	5648.15	2281.10	5225.52	2202.78	5105.34	1885.97	4616.37	
Wetland	10,628	40.93	95.70	35.99	87.23	34.89	85.44	30.57	78.70	
Construction land	15,349	67.92	156.63	58.97	141.58	56.95	137.94	50.26	126.94	
Unused land	324,477	584.14	1586.01	517.89	1462.67	502.54	1434.03	457.70	1355.01	
Total	1,161,626	5165.41	11177.82	4660.12	10369.79	4511.80	10139.85	3924.75	9255.84	

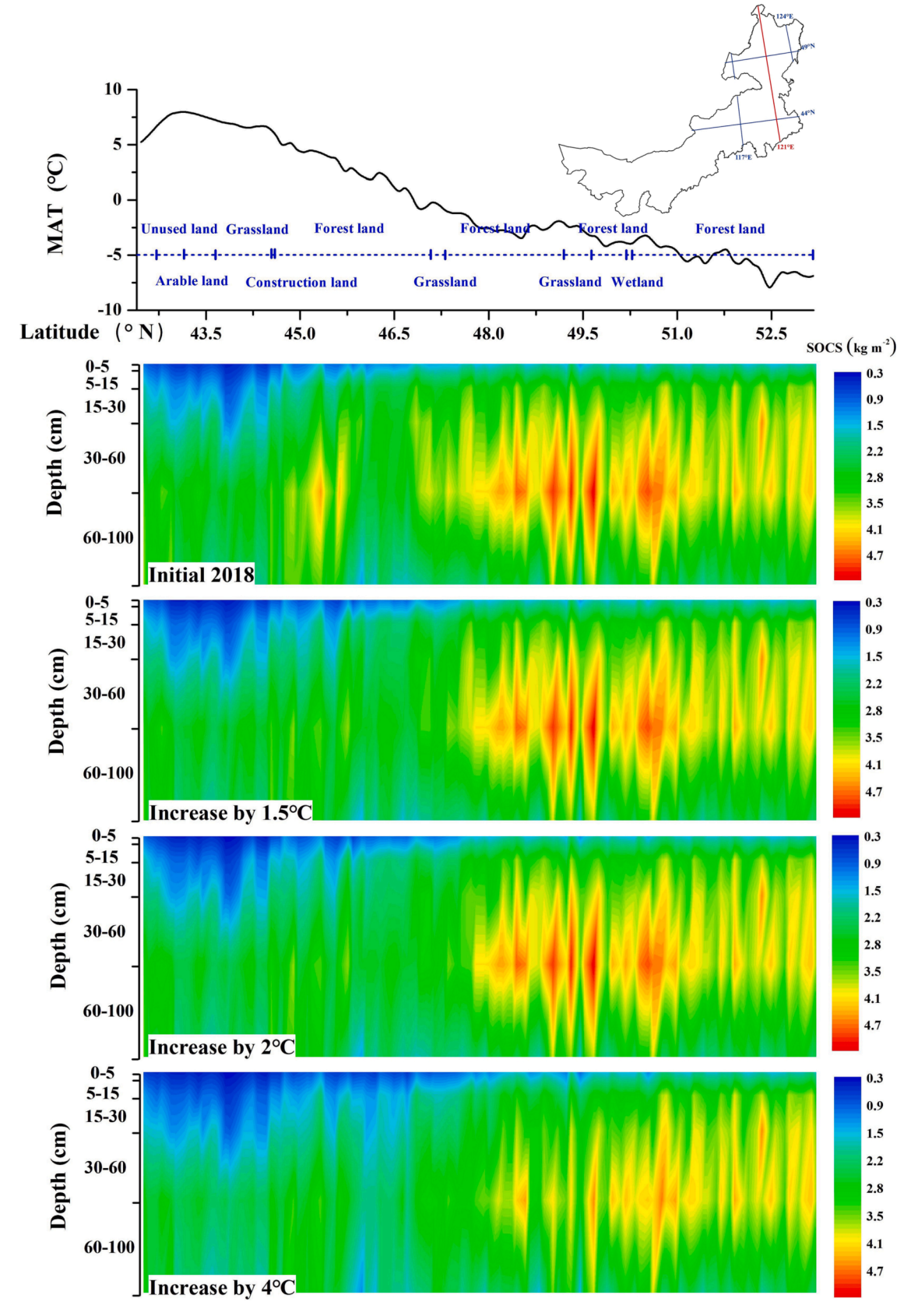


Fig. 6. Vertical distribution of soil organic carbon stocks at the top 1 m depth along longitude 121°E in response to climate warming.

#### 5. Conclusions

In this study, we have developed a combined of BRT model, ESF, and STS method to simulate the spatial variation of three-dimensional SOCS in response to climate warming in Inner Mongolia, China. This integrated model effectively simulates SOCS with higher LCCC and R<sup>2</sup> and lower RMSE and MAE. Under different climate warming scenarios, the spatial distribution of SOCS at various depths exhibited consistent patterns, with higher SOCS predominantly located in the northeast region and lower SOCS in the west region. The majority of SOCS was stored within the topsoil layer (0-30 cm), accounting for 46 % of total SOCS within a 1 m profile. With increasing the climate warming scenarios of 1.5 °C, 2 °C and 4 °C, there was a corresponding decrease in SOCS by approximately 7 %, 9 % and 17 %, respectively. The reduced SOCS were mainly distributed in grassland areas, accounting for approximately 50 % of the total reduction. NDVI, MAT and ELE were identified as primary variables influencing the three-dimensional spatial variation of SOCS. In summary, these findings provide fundamental data support for ecological restoration efforts, sustainable land use practices, and policy formulation related to land management in Inner Mongolia. Moreover, they had significance scientific implications for estimating grassland soil carbon stocks response to climate change while reducing uncertainties associated with its impact.

#### CRediT authorship contribution statement

Shuai Wang: Conceptualization, Investigation, Methodology, Writing – original draft. Xingyu Zhang: Data curation, Methodology. Kabindra Adhikari: Writing – review & editing. Zicheng Wang: Data curation, Methodology. Di Shi: Data curation, Methodology. Xinxin Jin: Funding acquisition, Investigation. Fengkui Qian: Writing – review & editing, Funding acquisition, Investigation.

#### **Declaration of Competing Interest**

The authors declare that they have no known competing financial interests or personal relationships that could have appeared to influence the work reported in this paper.

#### Data availability

The authors do not have permission to share data.

#### Acknowledgments

This work was funded by the National Key R&D Program of China (Grant No. 2021YFD1500200), National Natural Science Foundation of China (Grant No. 42077149), China Postdoctoral Science Foundation (Grant No. 2019M660782), Doctoral research start-up fund project of Liaoning Provincial Department of Science and Technology (Grant No. 2021-BS-136), Liaoning Provincial Department of Education General Project (LJKMZ20220996).

#### References

- Adams, S., Baarsch, F., Bondeau, A., Coumou, D., Donner, R., Frieler, K., ... Warszawski, L. 2013. Turn down the heat: climate extremes, regional impacts, and the case for resilience-executive summary.
- Adhikari, K., Hartemink, A.E., Minasny, B., Bou Kheir, R., Greve, M.B., Greve, M.H., 2014. Digital mapping of soil organic carbon contents and stocks in Denmark. PLoS One 9 (8), e105519.
- Adhikari, K., Owens, P.R., Libohova, Z., Miller, D.M., Wills, S.A., Nemecek, J., 2019.
  Assessing soil organic carbon stock of Wisconsin, USA and its fate under future land use and climate change. Sci. Total Environ. 667, 833–845.
- Aerenson, T., Tebaldi, C., Sanderson, B., Lamarque, J.F., 2018. Changes in a suite of indicators of extreme temperature and precipitation under 1.5 and 2 degrees warming. Environ. Res. Lett. 13 (3), 035009.

- Arrouays, D., McBratney, A. B., Minasny, B., Hempel, J. W., Heuvelink, G. B. M., MacMillan, R. A., McKenzie, N. J. 2014. The GlobalSoilMap project specifications. GlobalSoilMap: Basis of the global spatial soil information system.
- Arrouays, D., Leenaars, J.G., Richer-de-Forges, A.C., Adhikari, K., Ballabio, C., Greve, M., Rodriguez, D., 2017. Soil legacy data rescue via GlobalSoilMap and other international and national initiatives. GeoResJ 14, 1–19
- Bai, Y., Han, X., Wu, J., Chen, Z., Li, L., 2004. Ecosystem stability and compensatory effects in the Inner Mongolia grassland. Nature 431 (7005), 181–184.
- Bangroo, S.A., Najar, G.R., Achin, E., Truong, P.N., 2020. Application of predictor variables in spatial quantification of soil organic carbon and total nitrogen using regression kriging in the North Kashmir forest Himalayas. Catena 193, 104632.
- Batjes, N.H., 1996. Total carbon and nitrogen in the soils of the world. Eur. J. Soil Sci. 47 (2), 151–163.
- Berrang-Ford, L., Ford, J.D., Paterson, J., 2011. Are we adapting to climate change? Glob. Environ. Chang. 21 (1), 25–33.
- Bhunia, G.S., Kumar Shit, P., Pourghasemi, H.R., 2019. Soil organic carbon mapping using remote sensing techniques and multivariate regression model. Geocarto Int. 34 (2), 215–226.
- Bishop, T.F.A., McBratney, A.B., Laslett, G.M., 1999. Modelling soil attribute depth functions with equal-area quadratic smoothing splines. Geoderma 91 (1–2), 27–45.
- Blackburn, K.W., Libohova, Z., Adhikari, K., Kome, C., Maness, X., Silman, M.R., 2022. Influence of land use and topographic factors on soil organic carbon stocks and their Spatial and vertical distribution. Remote Sens. (Basel) 14 (12), 2846.
- Blois, J.L., Williams, J.W., Fitzpatrick, M.C., Jackson, S.T., Ferrier, S., 2013. Space can substitute for time in predicting climate-change effects on biodiversity. Proc. Natl. Acad. Sci. 110 (23), 9374–9379.
- Chen, S., Arrouays, D., Mulder, V.L., Poggio, L., Minasny, B., Roudier, P., Walter, C., 2022. Digital mapping of GlobalSoilMap soil properties at a broad scale: A review. Geoderma 409, 115567.
- Chen, W., Li, A., Hu, Y., Li, L., Zhao, H., Han, X., Yang, B., 2021. Exploring the long-term vegetation dynamics of different ecological zones in the farming-pastoral ecotone in northern China. Environ. Sci. Pollut. Res. 28, 27914–27932.
- Conrad, O., Bechtel, B., Bock, M., Dietrich, H., Fischer, E., Gerlitz, L., Böhner, J. 2015. System for automated geoscientific analyses (SAGA) v. 2.1. 4. Geoscientific Model Development, 8(7), 1991-2007.
- Dharumarajan, S., Hegde, R., 2022. Digital mapping of soil texture classes using Random Forest classification algorithm. Soil Use Manag. 38 (1), 135–149.
- Elith, J., Leathwick, J.R., Hastie, T., 2008. A working guide to boosted regression trees. J. Anim. Ecol. 77 (4), 802–813.
- Erbach, D.C., 1987. Measurement of soil bulk density and moisture. Trans. ASAE 30 (4), 922–0931.
- Eswaran, H., Van Den Berg, E., Reich, P., 1993. Organic carbon in soils of the world. Soil Sci. Soc. Am. J. 57 (1), 192–194.
- Fang, C., Smith, P., Moncrieff, J.B., Smith, J.U., 2005. Similar response of labile and resistant soil organic matter pools to changes in temperature. Nature 433 (7021), 57–59.
- Gibson, A.J., Hancock, G.R., Verdon-Kidd, D.C., Martinez, C., Wells, T., 2021. The impact of shifting Köppen-Geiger climate zones on soil organic carbon concentrations in Australian grasslands. Global Planet. Change 202, 103523.
- Gomes, L.C., Faria, R.M., de Souza, E., Veloso, G.V., Schaefer, C.E.G., Fernandes Filho, E. I., 2019. Modelling and mapping soil organic carbon stocks in Brazil. Geoderma 340, 337–350.
- Gray, J.M., Bishop, T.F., 2016. Change in soil organic carbon stocks under 12 climate change projections over New South Wales, Australia. Soil Sci. Soc. Am. J. 80 (5), 1296–1307
- Grimm, R., Behrens, T., Märker, M., Elsenbeer, H., 2008. Soil organic carbon concentrations and stocks on Barro Colorado Island—Digital soil mapping using Random Forests analysis. Geoderma 146 (1–2), 102–113.
- IPCC. 2006. 2006 IPCC Guidelines for National Greenhouse Gas Inventories, Prepared by the National Greenhouse Gas Inventories Programme, Eggleston H.S., Buendia L., Miwa K., Ngara T. and Tanabe K. (eds). Published: IGES, Japan.
- Jague, E.A., Sommer, M., Saby, N.P., Cornelis, J.T., Van Wesemael, B., Van Oost, K., 2016. High resolution characterization of the soil organic carbon depth profile in a soil landscape affected by erosion. Soil Tillage Res. 156, 185–193.
- Jobbágy, E.G., Jackson, R.B., 2000. The vertical distribution of soil organic carbon and its relation to climate and vegetation. Ecol. Appl. 10 (2), 423–436.
- Jones, C., McConnell, C., Coleman, K., Cox, P., Falloon, P., Jenkinson, D., Powlson, D., 2005. Global climate change and soil carbon stocks; predictions from two contrasting models for the turnover of organic carbon in soil. Glob. Chang. Biol. 11 (1), 154–166.
- Khalil, M.I., Kiely, G., O'Brien, P., Müller, C., 2013. Organic carbon stocks in agricultural soils in Ireland using combined empirical and GIS approaches. Geoderma 193, 222–235.
- King, A.D., Karoly, D.J., 2017. Climate extremes in Europe at 1.5 and 2 degrees of global warming. Environ. Res. Lett. 12 (11), 114031.
- Kumar, M., Kumar, A., Thakur, T.K., Sahoo, U.K., Kumar, R., Konsam, B., Pandey, R., 2022. Soil organic carbon estimation along an altitudinal gradient of chir pine forests in the Garhwal Himalaya, India: A field inventory to remote sensing approach. Land Degrad. Dev. 33 (17), 3387–3400.
- Lal, R., 2004. Soil carbon sequestration impacts on global climate change and food security. Science 304, 1623–1627.
- Lal, R., Kimble, J., Follett, R.F., 2018. Pedospheric processes and the carbon cycle. In: Soil Processes and the Carbon Cycle. CRC Press, pp. 1–8.
- Lamichhane, S., Kumar, L., Wilson, B., 2019. Digital soil mapping algorithms and covariates for soil organic carbon mapping and their implications: A review. Geoderma 352, 395–413.

- Lan, Z., Su, Z., Guo, M., Alvarado, C., Guo, F., Hu, H., Wang, G., 2021. Are climate factors driving the contemporary wildfire occurrence in China? Forests 12 (4), 392.
- Lin, L., 1989. A concordance correlation coefficient to evaluate reproducibility. Biometrics 45, 255–268.
- Malone, B.P., McPratney, A.B., Minasny, B., Laslett, G.M., 2009. Mapping continuous depth functions of soil carbon storage and available water capacity. Geoderma 154, 138-152
- Martin, M.P., Wattenbach, M., Smith, P., Meersmans, J., Jolivet, C., Boulonne, L., Arrouays, D., 2011. Spatial distribution of soil organic carbon stocks in France. Biogeosciences 8 (5), 1053–1065.
- Matejovic, I., 1993. Determination of carbon, hydrogen, and nitrogen in soils by automated elemental analysis (dry combustion method). Commun. Soil Sci. Plant Anal. 24 (17–18), 2213–2222.
- McBratney, A.B., Santos, M.L.M., Minasny, B., 2003. On digital soil mapping. Geoderma 117 (1–2), 3–52.
- McKenney, D.W., Pedlar, J.H., Papadopol, P., Hutchinson, M.F., 2006. The development of 1901–2000 historical monthly climate models for Canada and the United States. Agric. For. Meteorol. 138 (1–4), 69–81.
- Minasny, B., McBratney, A.B., Malone, B.P., Wheeler, I., 2013. Digital mapping of soil carbon. Advances in Agronomy. 118. Academic Press, pp. 1–47.
- Mishra, U., Lal, R., Slater, B., Calhoun, F., Liu, D., Van Meirvenne, M., 2009. Predicting soil organic carbon stock using profile depth distribution functions and ordinary kriging. Soil Sci. Soc. Am. J. 73 (2), 614–621.
- Mondal, A., Khare, D., Kundu, S., Mondal, S., Mukherjee, S., Mukhopadhyay, A., 2017. Spatial soil organic carbon (SOC) prediction by regression kriging using remote sensing data. Egypt. J. Remote Sens. Space Sci. 20 (1), 61–70.
- Mulder, V.L., Lacoste, M., Richer-De-Forges, A.C., Arrouays, D., 2016. GlobalSoilMap France: High-resolution spatial modelling the soils of France up to two meter depth. Sci. Total Environ. 573, 1352–1369.
- Nguemezi, C., Tematio, P., Silatsa, F.B., Yemefack, M., 2021. Spatial variation and temporal decline (1985–2017) of soil organic carbon stocks (SOCS) in relation to land use types in Tombel area, South-West Cameroon. Soil Tillage Res. 213, 105114.
- Olaya-Abril, A., Parras-Alcántara, L., Lozano-García, B., Obregón-Romero, R., 2017. Soil organic carbon distribution in mediterranean areas under a climate change scenario via multiple linear regression analysis. Sci. Total Environ. 592, 134–143.
- Reyes Rojas, L.A., Adhikari, K., Ventura, S.J., 2018. Projecting soil organic carbon distribution in central Chile under future climate scenarios. J. Environ. Qual. 47 (4), 735–745.
- Rezaei, S.A., Gilkes, R.J., 2005. The effects of landscape attributes and plant community on soil chemical properties in rangelands. Geoderma 125 (1–2), 167–176.
- Román-Sánchez, A., Vanwalleghem, T., Peña, A., Laguna, A., Giráldez, J.V., 2018. Controls on soil carbon storage from topography and vegetation in a rocky, semi-arid landscapes. Geoderma 311, 159–166.
- Shafizadeh-Moghadam, H., Minaei, F., Talebi-khiyavi, H., Xu, T., Homaee, M., 2022. Synergetic use of multi-temporal Sentinel-1, Sentinel-2, NDVI, and topographic factors for estimating soil organic carbon. Catena 212, 106077.
- Shahbazi, F., Hughes, P., McBratney, A.B., Minasny, B., Malone, B.P., 2019. Evaluating the spatial and vertical distribution of agriculturally important nutrients—nitrogen, phosphorous and boron—in North West Iran. Catena 173, 71–82.

- Siegenthaler, U., Wenk, T., 1984. Rapid atmospheric CO<sub>2</sub> variations and ocean circulation. Nature 308 (5960), 624–626.
- Smith, P., 2004. How long before a change in soil organic carbon can be detected? Glob. Chang. Biol. 10 (11), 1878–1883.
- Smith, P., Fang, C., Dawson, J.J., Moncrieff, J.B., 2008. Impact of global warming on soil organic carbon. Adv. Agron. 97, 1–43.
- Song, J., Gao, J., Zhang, Y., Li, F., Man, W., Liu, M., Li, C., 2022. Estimation of soil organic carbon content in coastal wetlands with measured VIS-NIR spectroscopy using optimized support vector machines and random forests. Remote Sens. (Basel) 14 (17), 4372.
- Strey, S., Boy, J., Strey, R., Weber, O., Guggenberger, G., 2016. Response of soil organic carbon to land-use change in central Brazil: a large-scale comparison of Ferralsols and Acrisols. Plant and Soil 408, 327–342.
- Tian, X.R., Shu, L.F., Zhao, F.J., Wang, M.Y., McRae, D.J., 2011. Future impacts of climate change on forest fire danger in northeastern China. J. For. Res. 22 (3), 437.
- Tsozué, D., Nghonda, J.P., Tematio, P., Basga, S.D., 2019. Changes in soil properties and soil organic carbon stocks along an elevation gradient at Mount Bambouto, Central Africa. Catena 175, 251–262.
- Tsui, C.C., Tsai, C.C., Chen, Z.S., 2013. Soil organic carbon stocks in relation to elevation gradients in volcanic ash soils of Taiwan. Geoderma 209, 119–127.
- Wang, S., Huang, M., Shao, X., Mickler, R.A., Li, K., Ji, J., 2004. Vertical distribution of soil organic carbon in China. Environ. Manag. 33 (1), S200–S209.
- Wang, S., Adhikari, K., Zhuang, Q., Gu, H., Jin, X., 2020. Impacts of urbanization on soil organic carbon stocks in the northeast coastal agricultural areas of china. Sci. Total Environ. 721, 137814.
- Wang, S., Zhou, M., Adhikari, K., Zhuang, Q., Bian, Z., Wang, Y., Jin, X., 2022. Anthropogenic controls over soil organic carbon distribution from the cultivated lands in Northeast China. Catena 210, 105897.
- Wu, T., Wang, D., Mu, C., Zhang, W., Zhu, X., Zhao, L., Wu, X., 2022. Storage, patterns, and environmental controls of soil organic carbon stocks in the permafrost regions of the Northern Hemisphere. Sci. Total Environ. 828, 154464.
- Yang, R.M., Zhang, G.L., Yang, F., Zhi, J.J., Yang, F., Liu, F., Li, D.C., 2016. Precise estimation of soil organic carbon stocks in the northeast Tibetan Plateau. Sci. Rep. 6 (1), 1–10.
- Zhang, Z., Ding, J., Zhu, C., Shi, H., Chen, X., Han, L., Wang, J., 2022b. Changes in soil organic carbon stocks from 1980–1990 and 2010–2020 in the northwest arid zone of China. Land Degrad. Dev. 33 (15), 2713–2727.
- Zhang, M., Shi, W., Ren, Y., Wang, Z., Ge, Y., Guo, X., Ma, Y., 2022a. Proportional allocation with soil depth improved mapping soil organic carbon stocks. Soil Tillage Res. 224, 105519.
- Zhao, F., Wu, Y., Hui, J., Sivakumar, B., Meng, X., Liu, S., 2021. Projected soil organic carbon loss in response to climate warming and soil water content in a loess watershed. Carbon Balance Manag. 16 (1), 1–14.
- Zhou, Y., Hartemink, A.E., Shi, Z., Liang, Z., Lu, Y., 2019. Land use and climate change effects on soil organic carbon in North and Northeast China. Sci. Total Environ. 647, 1230–1238.
- Zuo, Y., Serfling, R., 2000. General notions of statistical depth function. Ann. Stat. 461–482.